Appl. Math. Mech. -Engl. Ed., **00**(0), 1–27 (2019)

Applied Mathematics and Mechanics (English Edition)

https://doi.org/10.0000/s00000-000-0000-0

A numerical investigation of CO_2 dilution on the thermochemical characteristics of a swirl stabilized diffusion flame *

Shidvash Vakilipour[1,2,†], Yasaman Tohidi[1], Jafar Al-Zaili[3], Rouzbeh Riazi[1]

1. Faculty of New Sciences and Technologies, University of Tehran, North Kargar Street, Tehran, Iran;
2. Department of Mechanical Engineering, University of Manitoba, Winnipeg, MB R3T 5V6, Canada;
3. Department of Mechanical Engineering & Aeronautics, Northampton Square, London, EC1V 0HB

(Received / Revised)

The turbulent combustion flow modeling are performed to study the impacts of CO_2 addition to the fuel and oxidizer streams on the thermochemical characteristics of a swirl stabilized diffusion flame SM1. A flamelet approach along with three well-known turbulence models are utilized to model the turbulent combustion flow field. The k-ω SST shows the best agreement with the experimental fields compared to other methods. Then, the k–ω SST is employed to study the effects of CO_2 dilution on the flame structure and strength, temperature distribution, and CO concentration. To determine the chemical effects of CO_2 dilution, a fictitious species is replaced with the regular CO_2 in both fuel and oxidizer streams. The results indicate that the flame temperature is decreased when CO_2 is added to either fuel or oxidizer streams. The flame length reduction is observed at all levels of CO_2 dilution. The H radical concentration indicating the flame strength decreases following by the thermochemical effects of CO_2 dilution processes. In comparison with fictitious species dilution, chemical effects of CO_2 addition enhance CO mass fraction. The numerical simulations show that by increasing the

* Citation: Vakilipour, Shidvash and Tohidi, Yasaman and Al-Zaili, Jafar and Riazi, Rouzbeh. Title. *Applied Mathematics and Mechanics* (*English Edition*) (2019) https://doi.org/00.0000/s00000-000-0000-0

† Corresponding author, E-mail: vakilipour@ut.ac.ir

level of dilution the rate of flame length reduction is more significant at low swirl numbers.

Key words Swirl stabilized flame, CO_2 dilution, Methane-Air chemical effects, turbulent flame structure, steady flamelet model

1 Introduction

The ongoing depletion of fossil fuels, along with the global warming issue has become a significant concern in recent years. In this regard, two basic strategies are increasingly recognized to control this issue. Firstly, alternative fuels such as biogas and syngas, composed of up to 40% of diluents, are considered to replace the fossil fuels. Secondly, different new technologies have been proposed to control emission levels; e.g. oxy-fuel combustion technology for CO_2 Capture and Storage (CCS) [1], flameless combustion regimes [2], and Exhaust Gas Recirculation (EGR) [3]. The principle of both strategies is the dilution of reactants using different methodologies. Therefore, it is necessary to perform a precise study on the effects of diluent addition to fuel and oxidizer streams. To achieve this aim, the injection of CO_2 into either the fuel or oxidizer stream has been taken into consideration by several researchers. Since CO_2 is a combustion product, it can be easily extracted from the exhaust gas by condensing water vapor exists in the combustion products. Using CO_2 as a diluent has significant impacts on the flame structure, flammability limits, and pollutant emissions. Several researchers have investigated the effects of CO_2 dilution on the characteristics of different flames.

Liu et al. [4] depicted that the CO_2 addition to the fuel and oxidizer streams influences the flame structure through thermal and chemical effects in a laminar diffusion flame. They reported that the reaction $OH+CO=H+CO_2$ is mainly responsible for the chemical effects of CO_2 dilution. Erete et al. [5] experimentally considered the effects of CO_2 addition on the structure and pollutant emissions of turbulent diffusion flames. They found that with the higher diluent concentration in the fuel stream, visible flame length and flame temperature are reduced. Park et al. [6] performed a numerical simulation to study the impacts of CO_2 addition to the fuel and oxidizer streams on the flame structure of counter-flow diffusion flames. They had shown that the amount of radicals like H and OH is limited by addition of CO_2 to both reactant sides.

Mameri et al. [7] showed that the increase of CO_2 in biogas composition induces a decrease in the temperature, OH and H mass fractions. They also found that the chemical effects of CO_2 addition lead to the increase of CO and NO. Chen and Ghoniem [8] investigated the chemical effects of CO_2 dilution on CO formation for an oxy-fuel swirling flow diffusion flame. They depicted that CO mass fraction increases in high levels of CO_2 dilution. Glaborg and Bentzen [9] showed that in an oxy-fuel combustion system, the concentration of CO increases in the near burner regions. Hoerlle et al. [10] evaluated the effects of CO_2 addition to the fuel stream for a co-flow flame configuration. Their results depicted that a decrease in flame length, temperature, and CO mass fraction increases the volume rate of the diluent. The effect of CO_2 addition on the flame structure has been considered by some researchers. Cao et al. [11] studied the impacts of pressure and dilution of fuel side on co-flow diffusion flames. Both numerical and experiment results depicted that the flame length decreases by addition of diluent to the fuel stream in atmospheric pressure. Wilson and Lyons [12] investigated the effects of fuel stream dilution on the structure of turbulent diffusion flames. They argued that as the concentration of diluent increases, the flame shape becomes more cylindrical. Cao et al. [13] demonstrated that flame length is proportional to the mass flow rate of reactants in co-flow diffusion flames. Watanabe et al. [14] found out that the overall average length of oxy-flames is considerably shorter than that of air-flames in a swirl stabilized combustor. Furthermore, other researchers concluded that CO_2 dilution is an effective way to decrease pollutant emissions such as soot and NO_x [15, 16].

Other researchers compared the impacts of different diluents added to fuel or oxidizer streams. Park et al. [17] investigated the effects of different diluents in methane-air diffusion flames and showed that thermal effects of CO_2 addition lead to a reduction in flame temperature and NO_x emission. Zhuo et al. [18] conducted a numerical study on the impact of N_2, CO_2 and H_2O addition to fuel streams on combustion characteristics of syngas turbulent non-premixed jet flames. Their results demonstrated that the CO_2 diluted flame has the highest reduction in flame temperature amongst the other diluted flames. They had also shown that the CO_2 addition shortens flame size and provides the lowest extinction and re-ignition temperatures. Wang et al. [19] performed a numerical investigation on the physical and chemical impacts of CO_2 and H_2O dilution in the diffusion flames. They showed that the flame temperature is reduced due to thermal and chemical effects of CO_2 dilution. Also, The chemical effects of

CO_2 dilution increase the emission index of CO (EICO) while the thermal and dilution effects slightly reduce it. Min et al. [20] studied the effects of Ar, N_2 and CO_2 addition to the oxidizer stream on the flame length and lifting behavior of diffusion flames. They concluded that the pure dilution effect is a primary factor that affects the behavior of flame length. Xu et al. [21] investigated the effects of H_2O and CO_2 addition to the oxidizer stream and the characteristics of co-flow diffusion flames. They found that the chemical effects of CO_2 replacement of N_2 in the air stream, decrease OH and temperature followed by thermal effects.

Although the effects of CO_2 dilution have been considered on several research fronts, few studies have been done to investigate the effects of air swirl on the characteristics of CO_2 diluted flames. Swirling flames are commonly used in a wide range of engineering applications such as gas turbines and internal combustion engines [22]. These kinds of flames have several merits that justify their use. The fundamental significance of swirling flames is their role in increasing the degree of mixing between fuel and oxidizer, decreasing the flame length, improving flame stability, resulting in pollutant emission reduction [22, 23, 24, 25, 26]. A wide range of research has been conducted in the study of combustion characteristics of turbulent premixed [27, 28, 29], non-premixed [30, 31, 32, 33, 34] and partially premixed [35, 36] swirling flames. Beer and Chigier [37] proposed a non-dimensional swirl number to characterize the intensity of swirl in a swirling flow. It is defined as the ratio of the axial flux of angular momentum to the axial flux of axial momentum, but in this study a geometric swirl number s_g, which is the ratio of circumferential velocity to axial velocity is utilized to indicate the swirl intensity. The swirl number can be enhanced by the increasing of circumferential component of the velocity. The swirling flow is capable of generating turbulent recirculation zones complicating the flame structure. Generally the recirculation zone is established for swirl numbers greater than 0.5 [38]. In this situation, induced centrifugal forces create an adverse pressure gradient in the flow direction leading to the decrease of axial velocity, and finally, the flow direction becomes reversed. This causes the creation of a recirculation zone downstream of the burner [39]. The presence of a recirculation zone increases the residence time of reactants in the combustor which leads to a better mixing and a perfect reaction.

It is noteworthy to mention that the selection of an appropriate turbulence model plays a major role in the simulation of swirling flames. Some researchers focus on the numerical methods with reasonable calculation time and cost that are able to capture the main characteristics of

flow fields along with the distribution of major and minor species [40, 41, 42, 43, 44, 45]. In this regard, Reynolds-averaged Navier-Stokes (RANS) turbulence models have shown acceptable levels of accuracy in the prediction of main flow features, and their results for mean values are comparable with more complicated turbulence models like Large Eddy Simulation (LES) [46]. In the current study three different turbulence models including standard $k-\varepsilon$, $k-\varepsilon$ RNG (Re-Normalisation Group), and $k-\omega$ SST (shear stress transport) are utilized to study the effects of turbulence on the characteristics of Sydney swirl flame (SM1). k–ε RNG is recognized as a model which shows reasonable behavior for swirling flows which presents more accurate results compared to standard $k-\varepsilon$ [47]. $k-\omega$ SST provides good accuracy in adverse pressure gradients [48], and gives satisfactory results in the simulation of swirling flows [49, 50, 51].

In the section that follows, the computational domain is described, and then the combustion model and numerical procedure will be explained. In section 3, the results of numerical simulations are discussed. The numerical simulations are validated against the experimental data using three different turbulence models. Velocity profile, mixture fraction, temperature, and CO mass fraction are compared with the experimental results. In subsection 3.2, the thermal and chemical effects of CO_2 addition to either fuel or oxidizer stream on the flame structure, temperature distribution and CO concentration of Sydney swirl stabilized diffusion flame [30] are investigated. Furthermore, the study has been extended to consider the influence of swirl intensity (number) on the flame structure of fuel-diluted flames. The paper will be closed by a summery and conclusion in Section 4.

2 The numerical modeling

2.1 The computational domain and flow modeling

In the present study, the fuel, swirl air, and co-flow air streams are supposed to be provided by Sydney swirl burner placed inside a wind tunnel [30]. The wind tunnel drives a co-flow unswirled air stream through a surrounding duct with the square cross-section. Figure 1 illustrates schematic of last 50 mm of swirl burner, its surrounded air stream duct, and established reacting flow zone above burner exit plane. In this figure, U_j, U_s, W_s, and U_e are the fuel jet, swirl axial, swirl tangential, and the co-flow air stream velocities, respectively. As shown in Figure 1, a 60 mm diameter annulus provides the swirling pure air and encompasses the stream of a fuel jet

Table 1 Flow characteristics of Sydney swirl burner.

Case	Fuel	Oxidizer	$U_j(m/s)$	$U_s(m/s)$	$W_s(m/s)$	$U_e(m/s)$	Temperature (K)	Pressur
SM1	Methane	air	32.7	38.2	19.1	20.0	300	1013

and a ceramic bluff-body face. In other words, fuel and oxidizer are separated by a bluff-body which generates recirculation zones in the flow field [52]. The diameter of fuel jet stream and bluff-body surface is $d=3.6$ mm and $D=50$ mm, respectively.

Table 1 denotes SM1 case flow specifications injected into the reacting flow field by swirl burner and wind tunnel. Regarding the magnitudes of swirl flow components, the swirl number of case SM1 is $W_s/U_s=0.5$ which is categorized as a medium swirl number, and RANS turbulence models are capable to capture its main flow characteristics. Also, the Reynolds number of fuel jet, swirl air flow, and co-flow air streams are 7200 and 75900,and 46000 respectively.

In present numerical investigation, the flow field depicted in Figure 1 is modeled by a two-dimensional wedge-type configuration and shown in Figure 2. To achieve a fully developed flow condition, the inlet flow streams are extended $D=50$ mm upstream of the burner exit plane. As demonstrated in Figure 2, the computational domain of reacting zone has been extended 350 mm from the burner exit plane along the x axis. The fuel, swirling air, and co-flow air inflows are numerically modeled implementing inlet velocity condition at a section beyond burner exit plane shown as inlet section. The turbulence intensity of fuel jet, swirl air flow, and co-flow air streams is being recognized to be 5%. 4%, and 2% sequentially. At outlet and side sections, Dirichlet condition is applied to maintain a uniform fixed pressure at those boundaries during flow and combustion computations. Temperature is set to the constant value of 300 Kelvin in all inlet boundaries. The no-slip velocity, zero normal gradient temperature, and zero normal gradient pressure conditions are imposed on solid walls. For the near wall region, a wall treatment is utilized. The inlet, sides, and outlet planes of the computational domain are discretized by structured quadrilateral control volumes clustered near the burner exit plane.

2.2 Combustion model

From the combustion modeling perspective, different models have been used to validate the swirl flames. One of the promising models which are able to capture turbulence-chemistry interaction with an acceptable accuracy is the laminar flamelet model which has been utilized

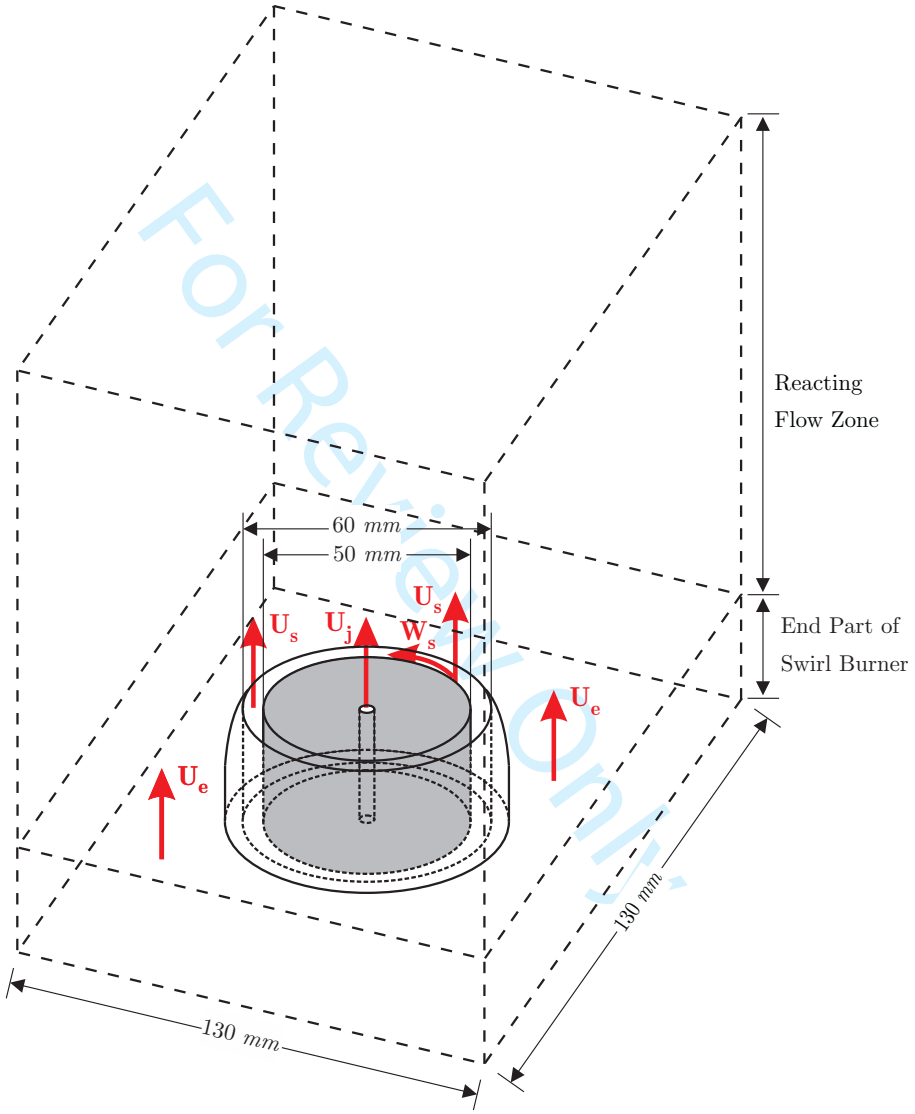

Fig. 1 The end part of Sydney swirl burner; fuel, swirl air, and coflow velocity directions and the dimensions of bluff-body and swirl air exit plane.

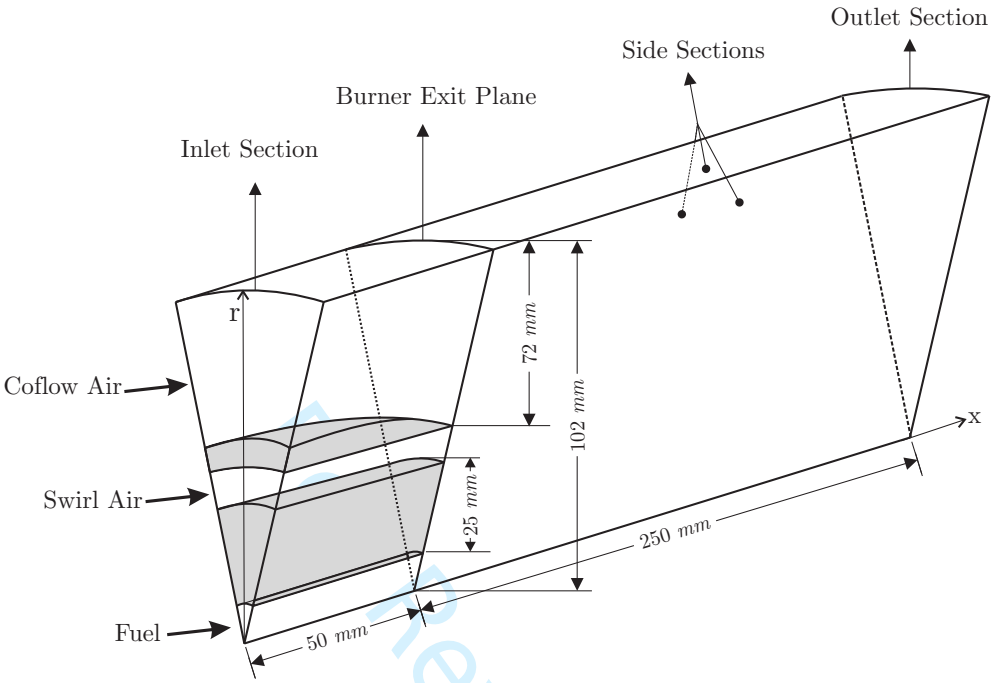

Fig. 2 The configuration of 2-D wedge-type computational domain.

by several well-known researchers [39, 53, 54]. In present work, the steady laminar flamelet model (SLFM) has been used to model the combustion process. SFLM considers the turbulent flames as a group of small laminar diffusion flames named flamelets. It is assumed that the chemical reaction zone is sufficiently thin with respect to the turbulent length scales [55]. One of the useful advantages of SLFM is that the flamelet calculations are independent from turbulent flow computations in the pre-processing step. In the pre-processing step, the flamelets are calculated and saved in the flamelet library tables, where the species mass fraction (Y_k) and the thermodynamic properties are obtained. The species mass fractions are calculated using mixture fraction (Z), its variance (Z'') and the scalar dissipation rate (χ). The mixture fraction measures the fuel/oxidizer ratio. It is set $Z = 0$ in the oxidizer stream and $Z = 1$ in the fuel stream. The scalar dissipation rate, χ, is regarded as an inverse diffusion time scale. Two governing equations for species mass fraction and temperature are written in mixture fraction space as follows:

$$\rho\frac{\partial Y_k}{\partial t} - \frac{1}{2}\rho\chi\frac{\partial^2 Y_k}{\partial Z^2} - \dot{\omega}_k = 0 \tag{1}$$

$$\rho\frac{\partial T}{\partial t} - \frac{1}{2}\rho\chi\left(\frac{\partial^2 T}{\partial Z^2} + \frac{1}{c_p}\frac{\partial c_p}{\partial Z}\frac{\partial T}{\partial Z}\right) + \frac{1}{c_p}\sum_{k=1}^{n} h_k\dot{\omega}_k = 0 \tag{2}$$

where ρ, T, and c_p denote density, temperature, and specific isobaric heat capacity, respectively. Density is characterized by ideal gas system. Also a polynomial parameterization is used to expresses the heat capacity as a fourth-order polynomial using two temperature ranges. Y_k, h_k, and $\dot{\omega}_k$ represent mass fraction, specific enthalpy, source term of chemical species k, respectively. A chemical reaction mechanism is used to calculate the chemical species source term $\dot{\omega}_k$. In steady laminar flamelet model, the mixture fraction along with the scalar dissipation rate at stoichiometric mixture fraction (χ_{st}) is utilized to define the flame structure. In the present study, the flamelets are computed via the open-source chemistry software Cantera [56]. Then the Favre presumed Probability Density Function (PDF) approach are used to estimate the mean species mass fraction and temperature.

$$\tilde{Y}_k = \int_0^\infty \int_0^1 Y_k\left(Z, \chi_{st}\right) P\left(Z, \chi_{st}\right) dZ d\chi_{st} \tag{3}$$

$$\tilde{T} = \int_0^\infty \int_0^1 T\left(Z, \chi_{st}\right) P\left(Z, \chi_{st}\right) dZ d\chi_{st} \tag{4}$$

Statistical independent assumption is utilized to decompose the joint PDF $P\left(Z, \chi_{st}\right)$.

$$P\left(Z, \chi_{st}\right) = P\left(Z\right) P\left(\chi_{st}\right) \tag{5}$$

The statistical independence separates the effects of large scale flow motions such as mixing (measured by mixture fraction Z) from small scale characteristics of flame such as local diffusion zone thickness (measured by scalar dissipation rate χ_{st}) [52]. A β-shape PDF and a simple Dirac function are employed for the mixture fraction distribution and the scalar dissipation rate, sequentially. Besides the flow motion and turbulence model equations, two other Favre averaged transport equations are discretized for the mixture fraction and its variance.

$$\frac{\partial \bar{\rho} \widetilde{Z}}{\partial t} + \frac{\partial \bar{\rho} \tilde{u}_i \widetilde{Z}}{\partial x_i} = \frac{\partial}{\partial x_i}\left(\mu_{eff} \frac{\partial \widetilde{Z}}{\partial x_i}\right) \tag{6}$$

$$\frac{\partial \bar{\rho} \widetilde{Z''^2}}{\partial t} + \frac{\partial \bar{\rho} \tilde{u}_i \widetilde{Z''^2}}{\partial x_i} = \frac{\partial}{\partial x_i}\left(\mu_{eff} \frac{\partial \widetilde{Z''^2}}{\partial x_i}\right) + 2\mu_{eff}\left(\frac{\partial \widetilde{Z}}{\partial x_i}\right)^2 - \bar{\rho}\widetilde{\chi} \tag{7}$$

Here, $u_i = (U, U_r)$ is the velocity component in the Cylindrical direction $x_i = (x, r)$, $\bar{\rho}$ is the time averaged density, and the effective viscosity μ_{eff} is the summation of molecular and eddy

viscosities, i.e. $\mu_{eff} = \mu + \mu_t$, where μ_t is calculated using a turbulence model. In Equation 7, the mean scalar dissipation rate $\tilde{\chi}$ is given by:

$$\tilde{\chi} = C_\chi \frac{\varepsilon}{k} \widetilde{Z''^2} \tag{8}$$

where $C_\chi = 2$ [57] and k and ε are the turbulent kinetic energy and dissipation rate, sequentially. In current SLFM, the chemical reaction mechanism applied for CH_4 combustion is GRI 2.11 with 49 species and 277 reactions [58]. Radiation heat transfer is also omitted.

2.3 Numerical procedure

Here, the flow and combustion computations are conducted utilizing Open source Field Operation And Manipulation (OpenFOAM) toolbox [59]. It is an open source CFD software package written by object-oriented C++ programming language and has been developed by OpenCFD Ltd at ESI Group and distributed by the OpenFOAM Foundation. Favre averaged Navier-Stokes and continuity equations are solved using Pressure-Implicit with Splitting of Operators (PISO) [60] algorithm to couple the pressure and velocity fields as well as Equation 6 and Equation 7 for mixture fraction and its variance, respectively. In the next step, $\tilde{\chi}$ is evaluated from $\widetilde{Z''^2}$, k, and ε. The mean temperature is determined by using probability density functions. Finally, density is calculated from temperature and pressure fields and utilized for flow computations in the next iteration. The convection and diffusion terms are discretised using central schemes with the second order of accuracy. The Courant number is set to the constant value of 0.3, and as a result, the time steps are small (about 2e-6 s). For achieving the solution convergence, two criteria were monitored. Firstly, the residuals of all variables drop below 10e-5. Secondly all the variables become stabilized and do not show any changes with iteration.

3 The results and discussion

In Figure 2, the axisymmetric two-dimensional computational domain were discretized using quadrilateral cells for current numerical experiments. To study the grid dependence of numerical solutions, the three different grid resolutions are adapted to perform flow field computations. The grid resolution is changed by varying its radial and the axial number of divisions. Table 2 denotes grid specifications utilized for grid independence numerical experiments. N_r and N_x

Table 2 The grid specifications generated for the grid study work of SM1 flame numerical simulation.

Grid	N_r	N_x	N_{cell}	N_{point}
Case 1	176	250	45950	92623
Case 2	251	299	79049	159060
Case 3	281	350	102330	205773

indicate the number of divisions in radial and axial directions, respectively. Figure 3 shows the profile of axial velocity for three grid resolutions in x=0.1m, which is a critical region due to the presence of secondary recirculation zone. As shown in this figure, the numerical results obtained from flow calculations on the grid with 79049 cells show a similar level of accuracy concerning those obtained on the grid with 102350 for all three turbulence models. Therefore, the grid with 79049 cells is employed to perform flow and combustion computations throughout the present study. The radial fuel inlet section, bluff-body surface, and swirl air plane are uniformly divided into partitions with $\Delta r = 0.06$, 0.21, and 0.25 mm, respectively. The wind tunnel coflow air section was non-uniformly discretized by 80 quadrilaterals clustered near the swirl air inlet section. In axial direction, the grid is spaced with $\Delta x = 0.64$ mm at the nozzle exit plane.

3.1 Validation

The numerical results obtained by present simulations are validated using experimental data provied by Al-Abdeli and Masri [30], Kalt et al. [32], and Masri et al. [34]. Figure 4 compares the calculated U velocity along the radial axis using three turbulence models with those of measurement at different x coordinates.

As shown in this figure, the numerical simulations follow the trend of experiment results. The negative values of U velocity at axial locations of $x/D = 0.136$ and 0.4 indicate the reverse flow pattern due to the presence of bluff-body surface which are captured well by all three turbulence models. The value of U velocity is over predicted around the center line At $x/D = 0.4$. It is because of the limited capability of Reynolds-averaged Navier-Stokes (RANS) models in shear flow computations which is mainly responsible for imprecise prediction of strong deceleration in the central jet flow. The downstream central recalculation zone which is due to the occurrence of vortex breakdown produces negative values on the center line at $x = 1.4$. Although standard k–ε is not able to capture the downstream recirculation zone, both k–ω SST and k–ε RNG

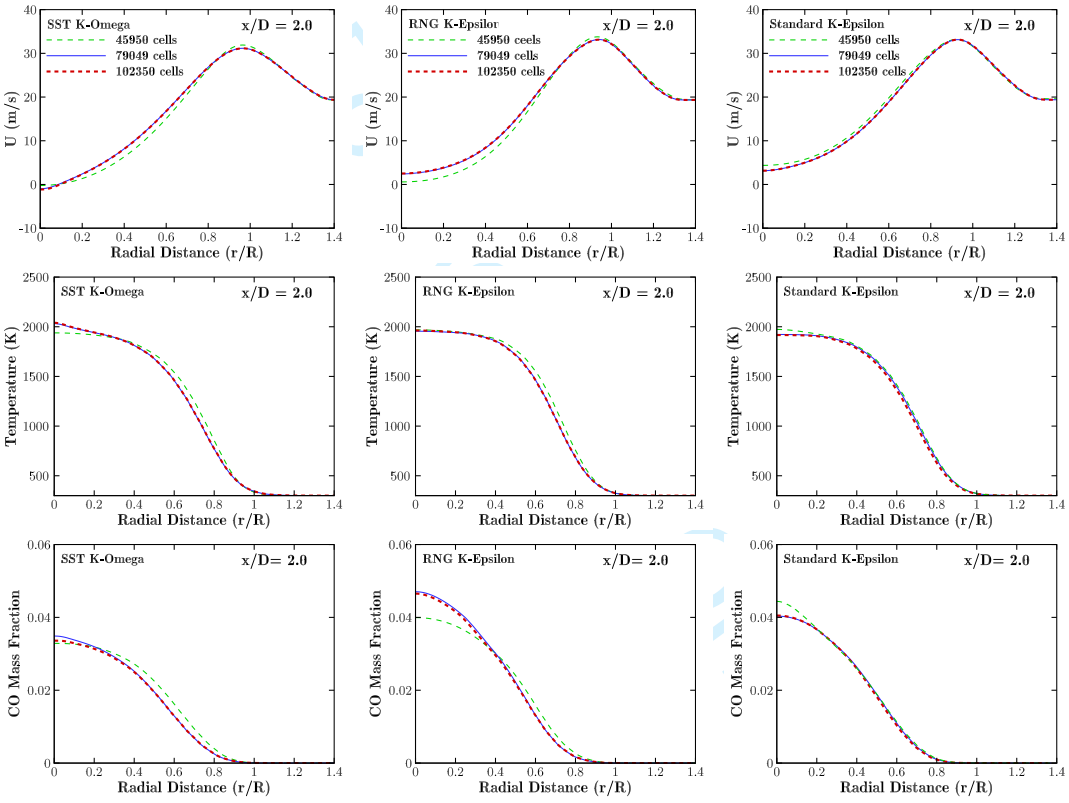

Fig. 3 Grid sensitivity study of the predicted axial velocity, temperature, and CO mass fraction for three distinct turbulence models.

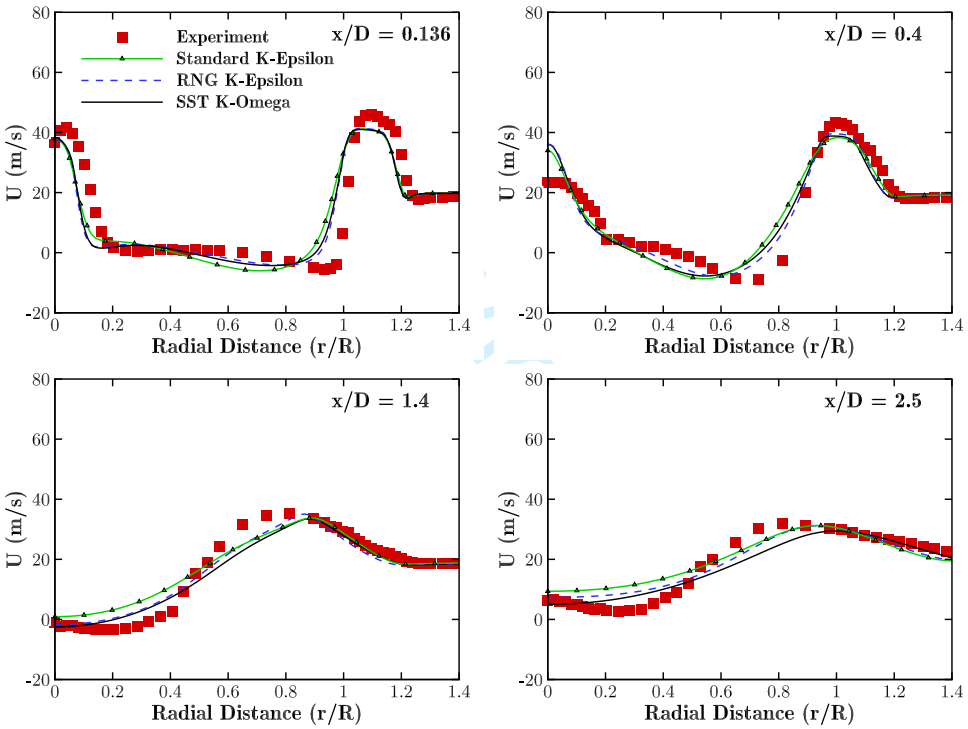

Fig. 4 Radial profile of the predicted axial velocity component compared with measurements at different axial locations.

models predict the rotating flow in this region with the acceptable accuracy.

Figure 5 shows predicted mixture fraction alongside those of experimental data at axial locations of $x/D = 0.2$, 1.1, 1.5, and 3. In this figure, k–ε RNG model overestimates the mixture fraction around the fuel jet centerline at axial flame locations from $x = 0.2$ to 1.5. This theme emerges that the turbulence flow calculations using k–ε RNG model within the high shear region around fuel jet core leads to an estimation of longer distance for fuel jet flow diffusion. On the other hand, the result of k–ω SST matches well with experiment results at the aforementioned axial locations. All three turbulence models predict the amount of mixture fraction less than measurements in regions near the bluff-body surface, i.e., at $x/D = 0.2$ and for radial distances more than $r/R = 0.06$. This is because the turbulence models cannot capture precession of central jet and show a straight flow movement which causes a redistribution of fuel from the jet to upstream recirculation zone. This trend has been also observed in LES simulation of swirling flames [39]. The underestimation of mixture fraction makes its profile to be close to its stoichiometric values. The stoichiometric mixture fraction is an indicator of the flame front where the computed flame temperature reaches its maximum value. Therefore, it is anticipated that the temperature distribution would be over-predicted in regions near the bluff-body surface. However, the results related to k–ω SST in this region show the higher level of accuracy compared with two other turbulence models.

Figure 6 shows comparisons for the radial profiles of the temperature field at different axial locations. All turbulence models show a discrepancy in the region near to burner exit plane ($x/D = 0.2$) which is due to the underestimation of mixing field. In other axial locations the results are comparable with the results of LES reported by Malalasekera et al. [53]. Since the temperature distributions at downstream locations are closely related to the mixture fraction predictions, k–ω SST shows the best prediction of temperature field in all axial locations.

The comparison of CO mass fraction with experiment results at different axial locations are shown in Figure 7. CO profiles are congruent with temperature results with similar trends and peaks. There is a significant under prediction of CO in the region near the bluff-body surface for k–ε RNG method. This is because the mixture fraction distribution is close to the lean flammability limit of the mixture for this model, so a considerable effect on the CO profile is observed in this region. CO concentration is well predicted at downstream axial locations by all three methods.

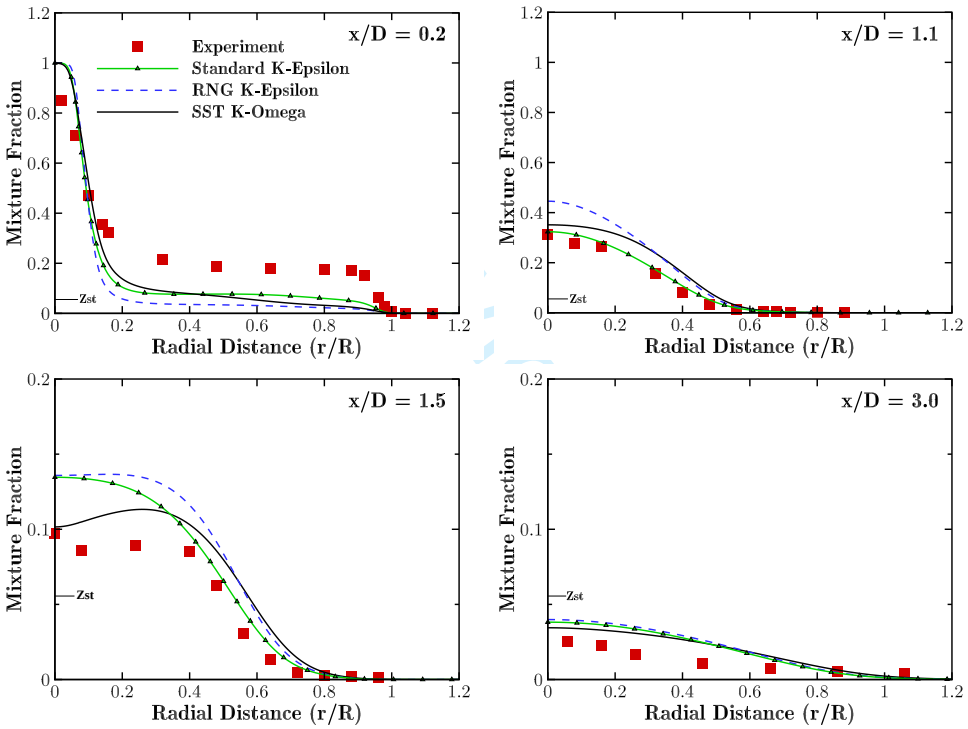

Fig. 5 Radial profile of predicted mixture fraction compared with measurements at different axial locations.

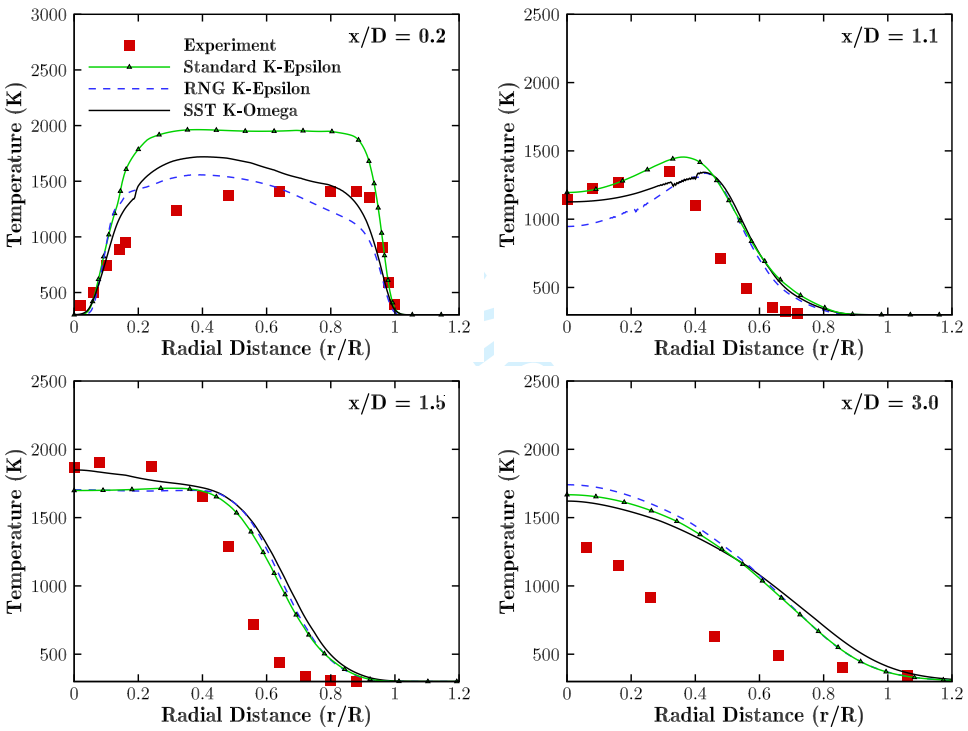

Fig. 6 Radial profile of predicted temperature distribution compared with measurements at different axial locations.

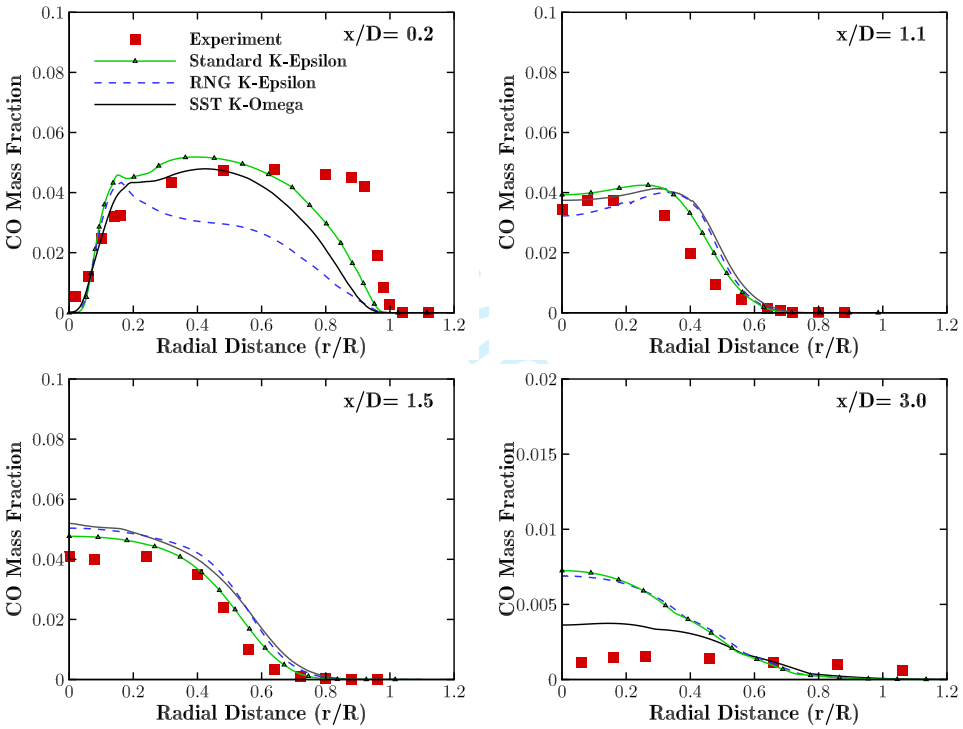

Fig. 7 Radial profile of predicted CO mass fraction compared with measurements at different axial locations.

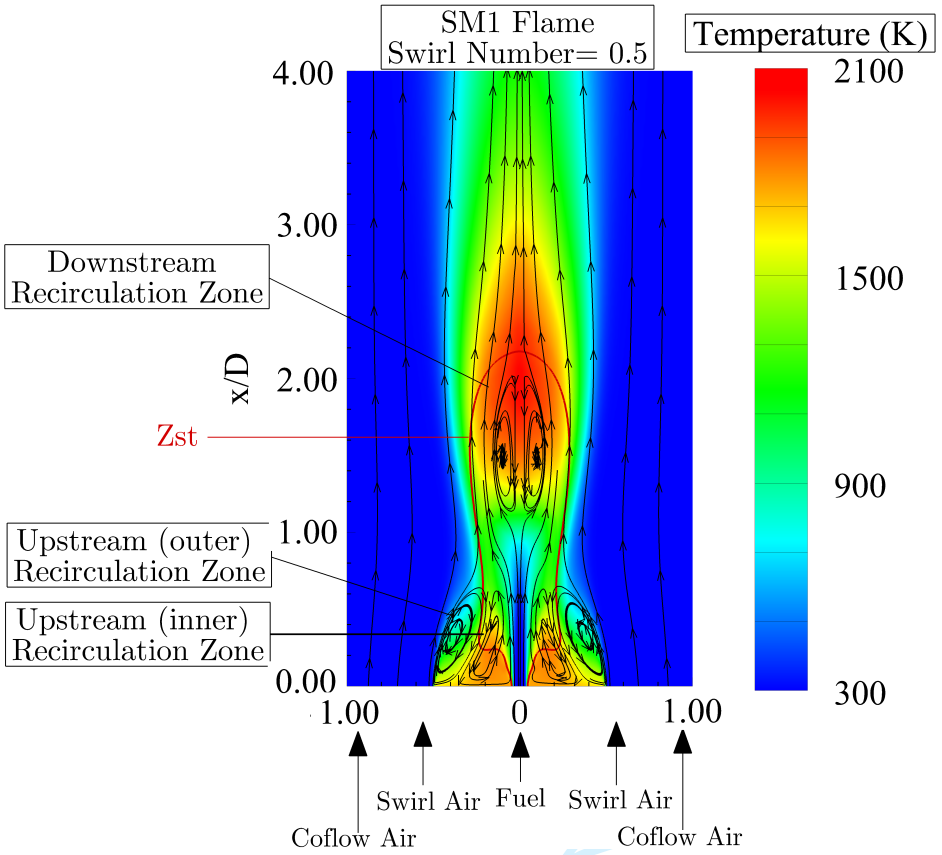

Fig. 8 The predicted structure of SM1 flame.

In summary, k–ω SST shows more satisfactory results compared with the two other methods. In fact this model is recognized as a model which is capable to present acceptable predictions in regions with adverse pressure gradients. Therefore, in this study k–ω SST is utilized for investigating the combustion characteristics of Sydney swirl flame (SM1).

The structure of swirl flames is too complicated; hence, the precise computation of flow field is a prominent factor in their numerical simulations. The computed flow streamlines patterns and temperature contours of SM1 are depicted in Figure 8. As is seen, two recirculation zones are resolved and emerged adjacent to bluff-body surface (upstream) and the one at downstream of the burner. The rotating gas zones resulting in a negative axial velocity lead to form a collar-like flow feature in the flame structure [30]. Moreover, the combustion products are trapped within the high-temperature zones predicted above the bluff-body and in the downstream re-circulation region. In these zones, the hot gases provide a continual source of ignition for the

Table 3 Non-dimensionalized flame length in different cases of fuel or oxidizer dilution.

Case	Fuel	Oxidizer	Z_{st}	L/D	Swirl Number
Case 1	CH_4	$79\%N_2+21\%O_2$	0.055	2.18	0.5
Case 2	$90\%CH_4+10\%CO_2$	$79\%N_2+21\%O_2$	0.071	2.03	0.5
Case 4	$80\%CH_4+20\%CO_2$	$79\%N_2+21\%O_2$	0.089	1.93	0.5
Case 5	CH_4	$10\%CO_2+69\%N_2+21\%O_2$	0.053	2.09	0.5
Case 7	CH_4	$20\%CO_2+59\%N_2+21\%O_2$	0.050	2.02	0.5
Case 8	CH_4	$79\%N_2+21\%O_2$	0.055	4.41	0.3
Case 8	$90\%CH_4+10\%CO_2$	$79\%N_2+21\%O_2$	0.071	3.80	0.3
Case 9	$80\%CH_4+20\%CO_2$	$79\%N_2+21\%O_2$	0.089	3.28	0.3
Case 10	CH_4	$79\%N_2+21\%O_2$	0.055	2.80	0.6
Case 10	$90\%CH_4+10\%CO_2$	$79\%N_2+21\%O_2$	0.071	1.76	0.6
Case 11	$80\%CH_4+20\%CO_2$	$79\%N_2+21\%O_2$	0.089	1.68	0.6

incoming fuel and therefore, enhances the flame stability.

3.2 Dilution effects

The effects of CO_2 dilution on the combustion characteristics of the bluff-body swirl stabilized diffusion flame SM1 are studied by increasing the concentration of CO_2 in fuel and oxidizer streams up to 20%. Table 3 denotes the specifications of the cases considered to study the influences of CO_2 dilution. In case of dilution modeling, the molar fraction of O_2 in the air stream is constant whereas the composition of fuel and oxidizer varies by replacement of CH_4 and N_2 with CO_2. L/D is the flame length (L) non-dimensionalized by bluff-body diameter (D). Flame length is one of the prominent parameters describing the structure of diffusion flames. There are different definitions for non-premixed turbulent flame length (L). In some instances, it is determined based on the visible flame length that has been proposed in experimental studies [5]. The other definition is that the flame length would be at the axial location of peak temperature on the centerline [21]. Another definition states that the flame length is considered as the axial distance on the centerline where the mixture fraction reaches its stoichiometric value. Since current studied flame structure has an hourglass shape in higher swirl numbers (s_g=0.6), the furthermost point of stoichiometric mixture fraction is not always on the centerline. In this regard, the flame length is defined as the highest axial distance between the fuel exit plane (bluff-body surface) and the place where the mixture fraction reaches to its stoichiometric ratio [41].

As denoted in Table 3, in a constant swirl number of 0.5, the non-dimensional flame length is

reduced gradually by addition of CO_2 to the fuel stream. Compared to the no diluted case, the flame length decreases about 7% and 11.5% in the case of 10% and 20% dilution respectively. Considering the molar weight of CO_2 and CH_4, the density of CO_2 is higher than of CH_4. Since a fixed volumetric flow rate is set at inlet boundaries, the addition of CO_2 to the fuel stream increases the mass flow rate of fuel jet, and therefore, an increment in flame length is expected. On the other hand, adding CO_2 to the fuel stream decreases combustible components of fuel which leads to the reduction of mixing time and the time needed for combustion of the fuel, so the flame is formed in the region closer to the exit plane. The similar result is observed in different studies for methane-air diffusion flames diluted by CO_2 [5, 18].

Similarly, the flame length is reduced with the addition of CO_2 to the oxidizer stream but, with a lower rate in comparison with the fuel stream dilution case. Compared to the no diluted case, the flame length decreases about 4% and 7.5% in the case of 10% and 20% dilution respectively. In the case of oxidizer stream dilution (i.e., replacement of N_2 by CO_2), the density of the oxidizer and consequently, its stream momentum increases. An increase in the momentum of the oxidizer flow results in the generation of stronger recirculation zones within the flow field which increases the level of fuel-oxidizer mixing. As a result, the flame length decreases due to increment of fuel-oxidizer mixing.

The effects of CO_2 dilution, imposed to either fuel or oxidizer stream, on the flame characteristics can be investigated considering three perspectives. Firstly, the dilution process reduces the combustible components which affect the flame characteristics. Secondly, the high heat capacity of diluent results in thermal effects leading to flame characteristics changes. Thirdly, the participation of diluent in chemical reactions results in chemical effects on the combustion characteristics [6].

Figure 9 demonstrates the radial temperature profiles at axial locations of $x/D = 0.2$, 1.1, 1.5, and 3.0 in the case of CO_2 addition to the fuel stream. It is observed that the increase of diluents molar concentration leads to the flame temperature reduction in all axial locations. With the higher concentration of CH_4, the increased breakage of exothermic bonds of carbon atoms in the hydrocarbon fuel leads to higher flame temperature. The lower amount of reactive species along with the high heat capacity of CO_2 reduces the flame temperature. Additionally, chemical effects of CO_2 dilution affect temperature distribution. The primary factor involved in the chemical effects of CO_2 is the thermal dissociation of CO_2 which is an endothermic

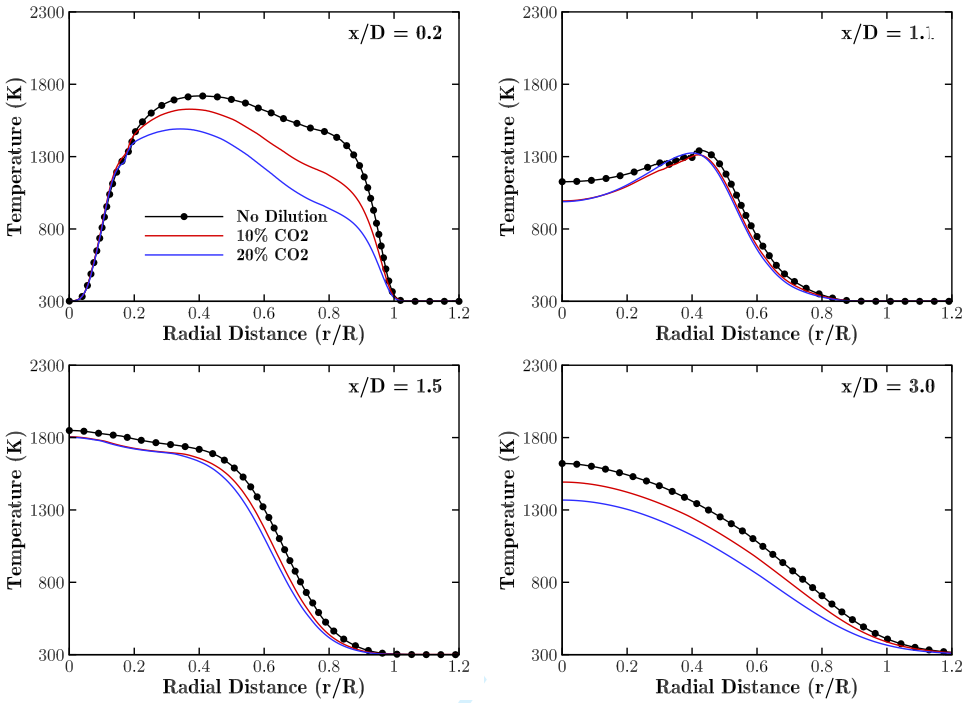

Fig. 9 Radial profile of predicted Temperature in the case of no dilution, 10% dilution and 20% dilution of the fuel stream at different axial locations.

process, the high concentration of CO_2 leads to the flame temperature reduction. The largest temperature reduction is seen in the region near the bluff-body surface ($x/D=0.2$) in which the temperature decreases about 498 K for 20% CO_2 diluted fuel case. As shown in Figure 9, by addition of CO_2 to the fuel stream, the maximum flame temperature moves toward the fuel-rich side. For instance, maximum flame temperature gets about 16% closer to the fuel rich side of the flame at the axial location of $x/D=1.1$ when 20% CO_2 is added to the fuel stream. It can be explained by the position of stoichiometric mixture fraction (from 0.055 in no dilution to 0.089 in 20% CO_2 dilution case) which is an indicator for the flame front. The increment of CO_2 alters the flame stoichiometry and as a result, dislocates the profile of temperature in the direction of fuel side.

In Figure 10, the temperature profiles at axial locations of $x/D=0.2$, 1.1, 1.5, and 3.0 are shown for the case of CO_2 addition to the oxidizer stream (replacement of N_2 by CO_2). Besides the higher heat capacity of CO_2 with respect to N_2, the chemical effects of CO_2 addition lead to the reduction of flame temperature. The maximum temperature reduction near the bluff-body surface is about 276 K in the case of 20% CO_2 addition to the oxidizer stream compared

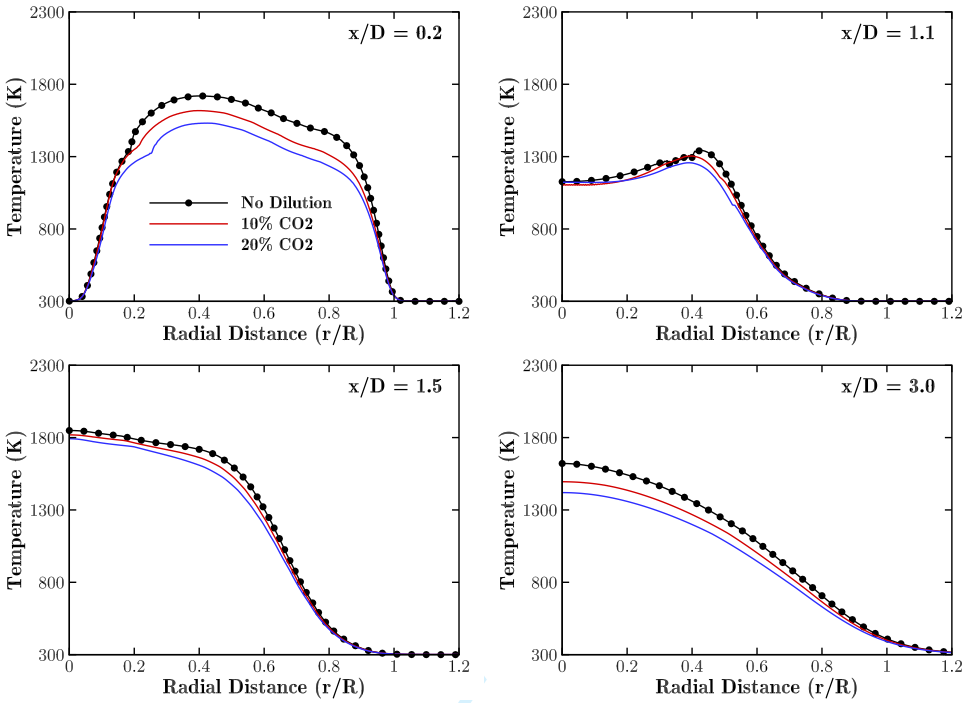

Fig. 10 Radial profile of predicted Temperature in the case of no dilution, 10% dilution and 20% dilution of the oxidizer stream at different axial locations.

to non diluted case. As shown in Figure 9 and Figure 10, the flame temperature reduction is more noticeable when the diluent is added to the fuel stream. It can be related to the constant thermal power of combustion system in case of oxidizer dilution. The reduction in radial temperature distribution at $x/D = 1.5$, is less than other axial locations for both fuel and oxidizer stream dilutions. This is because in both dilution cases the zone with maximum temperature at downstream is predicted to be placed closer to the upstream recirculation zones. Moreover the dilution effects decrease the flame temperature in the flow field. Hence, in this axial location, which is the closest section to the downstream recirculation zone, the temperature changes is less noticeable. Maximum flame temperature reduction due to the addition of 20% CO_2 is about 200 and 130 K for the fuel and oxidizer dilution cases respectively.

Chemical effects of dilution also have a significant impact on the species mass fraction. In order to study the chemical effects of CO_2 addition, a fictitious species FCO_2 is introduced [4] with the same thermal and transport properties of CO_2. On the other hand, FCO_2 does not participate in chemical reactions. According to this methodology, FCO_2, as an inert species, is added to fuel or oxidizer stream rather than regular CO_2. The differences between the results

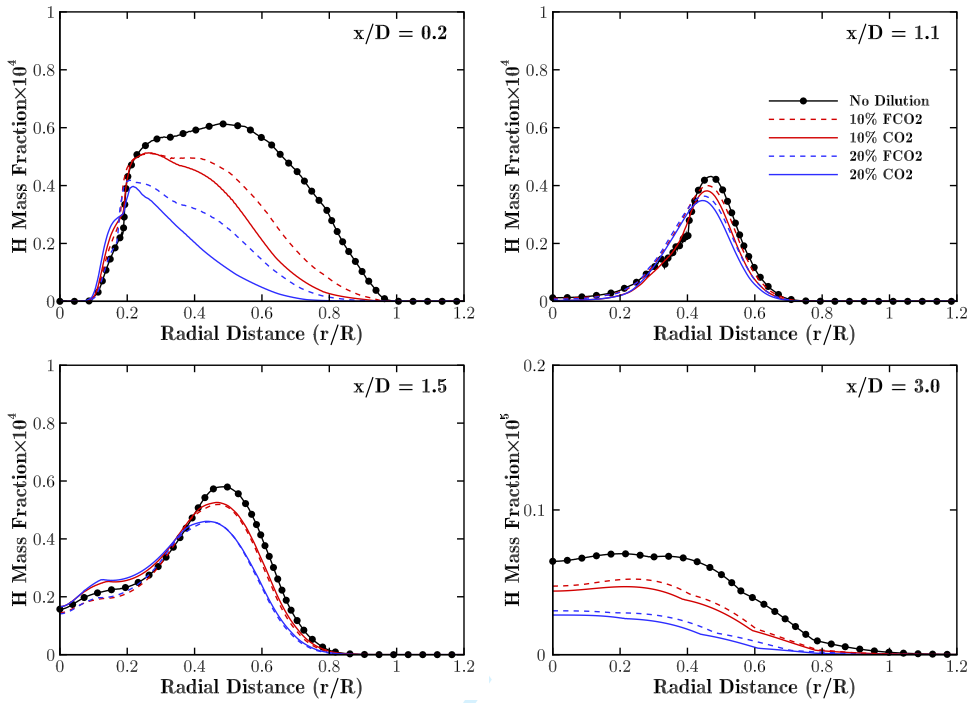

Fig. 11 Radial profile of calculated H radical mass fraction in the case of no dilution, 10% dilution and 20% dilution of fuel stream at selected axial locations.

of CO_2 and FCO_2 dilution can determine the chemical effects of CO_2.

Figure 11 and Figure 12 depict the profiles of computed H mass fraction at selected axial locations ($x/D = 0.2$, 1.1, 1.5, and 3.0) in the case of CO_2 and FCO_2 addition to the fuel and oxidizer streams, respectively.

The flame strength can be assessed by the concentration of radicals such as H and OH [6] which their amount is expected to be more at higher temperatures. The comparison between FCO_2 and CO_2 dilution reveals that both thermal and chemical effects of diluent addition decrease H mass fraction in all axial locations. In methane combustion system, four reactions have the most impacts on the flame characteristics because of their high rates [10]. The reaction

$$H+O_2 = O+OH \qquad R38$$

$$OH+H_2 = H+H_2O \qquad R84$$

$$H+CH_4 = CH_3+H_2 \qquad R53$$

$$OH+CO = H+CO_2 \qquad R99$$

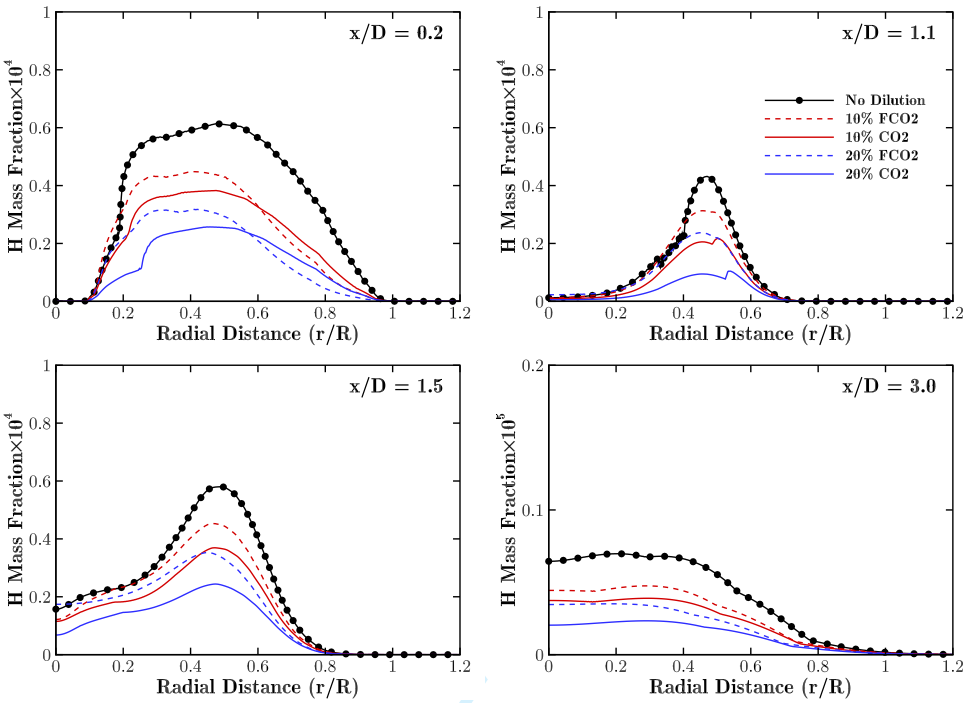

Fig. 12 Radial profile of calculated H radical mass fraction in the case of no dilution, 10% dilution and 20% dilution of the oxidizer stream at selected axial locations.

numbers are similar to the sequence in GRI-Mech 2.11. The reaction R99 is introduced as the main reaction responsible for the chemical effects of CO_2 dilution by several authors [4, 6, 8, 10]. As the fuel is diluted by CO_2 species, reaction R99 starts to consume H atoms. On the other hand, the reaction R38 and R53 are competing for the H atoms in the oxidizer and fuel sides, respectively. These reactions reduce their rates and consequently diminish the H_2 and OH production. As a result, the reaction R84 is affected, and it leads to a further decrease of the H radicals. OH concentration is also reduced by addition of CO_2 to the fuel and oxidizer streams. It is the direct result of H atoms consumption in reaction R99 which suppress reaction R38. As depicted in Figure 11 and Figure 12, comparing the results of CO_2 dilution with FCO_2 dilution reveals that the chemical effects of CO_2 dilution are more noticeable when CO_2 is added to the oxidizer stream. For instance, the maximum reduction of H radicals due to the chemical effects of CO_2 addition is about 10% for both 10% and 20% fuel dilution cases at the axial location of $x/D = 0.2$. However, the chemical effects decrease maximum H radical concentration about 17% and 33% at the same axial location in the case of 10% and 20% oxidizer dilution respectively. This is because in higher flame temperature(see Figure 9 and

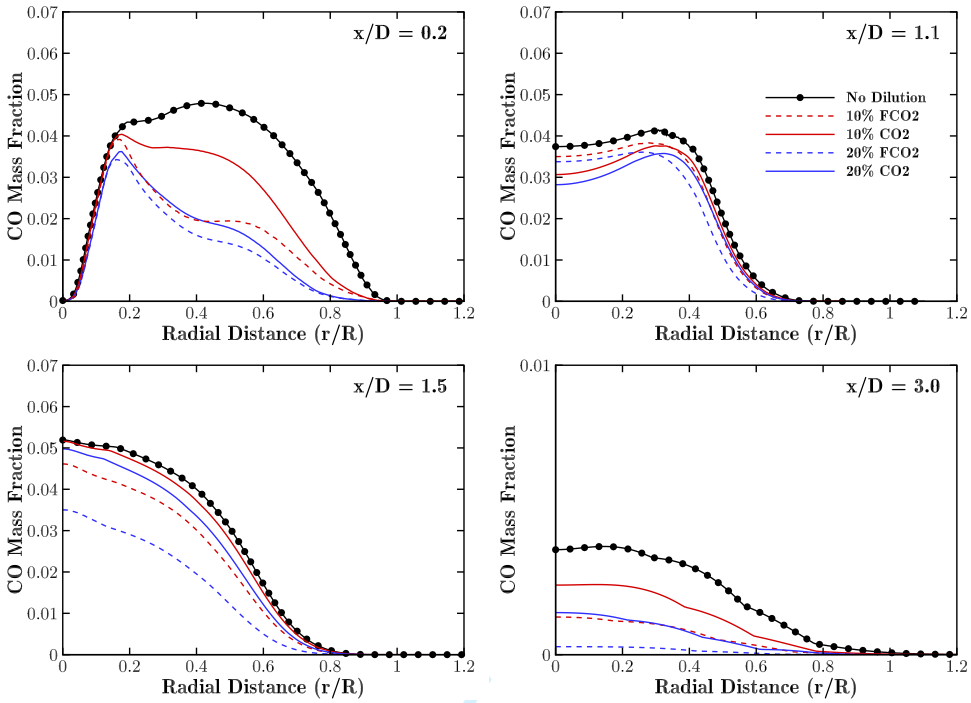

Fig. 13 Radial profile of predicted CO mass fraction in the case of no dilution, 10% dilution and 20% dilution of fuel stream at selected axial locations.

Figure 10), the thermal dissociation of CO_2 is much easier. Since the flame length varies in different cases, it is difficult to compare the fuel and oxidizer dilution effects at an axial location far from the exit plane.

Figure 13 depicts the profiles of computed CO mass fraction for the fuel CO_2 and FCO_2 dilutions in radial direction at $x/D = 0.2$, 1.1, 1.5, and 3.0. As can be seen in this figure, CO mass fraction decreases when CO_2 is added to the fuel stream in all axial locations. The difference between CO_2 and FCO_2 dilution cases confirms that the chemical effects of diluent addition to the fuel stream lead to the increase of CO mass fraction. It is important to mention that the produced CO mass fraction depends highly on the CO_2 mass fraction, H mass fraction and, flame temperature distribution [6]. As previously noted, in the case of fuel stream dilution, the temperature is much lower compared with the oxidizer stream dilution case. It is worth mentioning that the production of CO originates from CO_2 breaking down by thermal dissociation process. In this regard, even though the CO_2 concentration increases in the fuel stream, the produced CO mass fraction is low due to low flame temperature. On the other hand, the production of CO is limited by the reduction of H radical concentration. The rate of

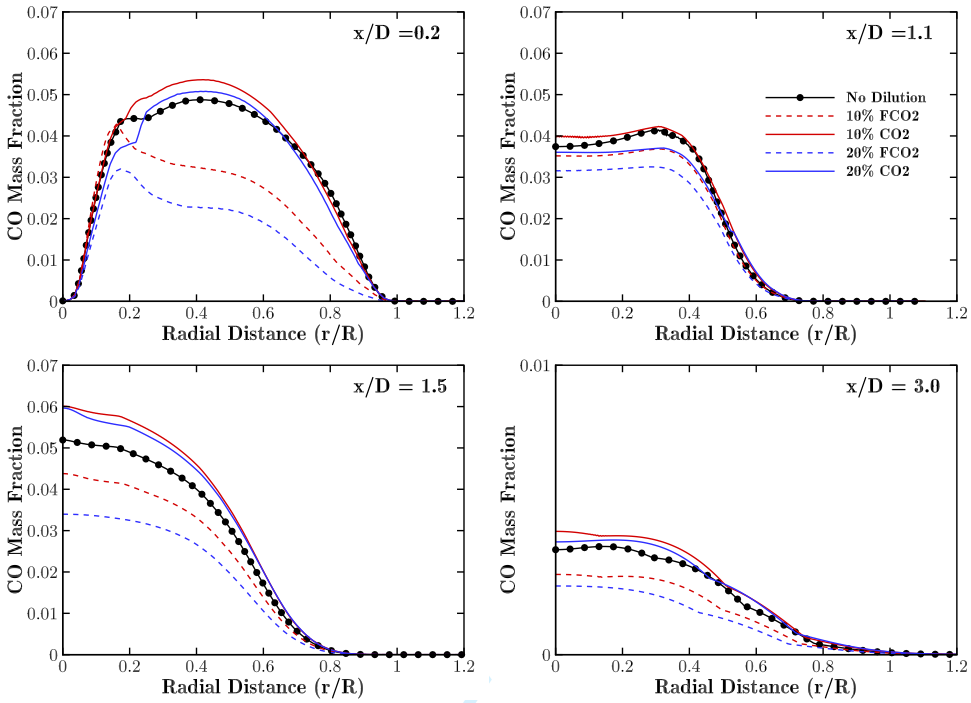

Fig. 14 Radial profile of predicted CO mass fraction in the the case of no dilution, 10% dilution and 20% dilution of oxidizer stream at selected axial locations.

reduction is minimum at the axial location of $x/D=1.5$ because the high temperature (about 1850 K) and the high amount of H radical increase the production of CO compared to other axial locations. Maximum reduction rate of CO is about 6% and 14% for 10% and 20% fuel dilution cases respectively at $x/D = 1.5$. Also the chemical effects of CO_2 addition increase CO concentration about 13% and 40% for 10% and 20% diluted fuel respectively at the same location.

Figure 14 depicts the profiles of CO mass fraction computed for the oxidizer CO_2 and FCO_2 dilution cases in radial direction at $x/D=0.2$, 1.1, 1.5, and 3.0. In the case of oxidizer dilution, higher flame temperature contributes to the thermal dissociation of CO_2, so in the locations with a high H mass fraction, the production of CO is considerably increased in the case of 10% CO_2 addition at all axial locations (see Figure 14). The concentration of CO decreases slightly in the case of 20% CO_2 dilution compared to 10% CO_2 dilution because the low flame temperature limits the thermal dissociation of CO_2. The maximum increasing of CO concentration is seen at $x/D=1.5$ which is about 16% for both dilution cases. The chemical effects of CO_2 addition is also more pronounced at $x/D = 1.5$ compared to other axial locations (due to the higher

flame temperature), and it increases about 40% and 81% for the cases of 10% and 20% oxidizer dilution respectively.

To study the influence of fuel dilution and swirl intensity interactions on the flame structure, the CO_2 dilution of fuel stream with 10% and 20% CO_2 molar concentration is performed at the swirl number of 0.3 and 0.6. Figure 15 shows predicted temperature contours within the flow with 0%, 10% and 20% fuel dilution and at air swirl numbers of 0.3 and 0.6.

In swirl number of 0.3, a conical shape at the downstream position is formed in which the maximum flame temperature is located on the centerline of the nozzle. Correspondingly, at swirl number of 0.6, the flame has an hour-glass shape with sharp edges. In the undiluted case, the flame length is 36% longer at swirl number of 0.3 compared to swirl number of 0.6. Also the flame radius is smaller (about 10%) at the swirl number of 0.3. This is because, in low tangential velocities, the momentum of oxidizer decreases and the fuel stream penetrates more in the downstream. Conversely, in stronger swirl intensities (swirl number of 0.6), the adverse pressure gradient leads to flame length reduction. By the addition of CO_2 to the fuel stream, the length and radius of high temperature regions are reduced in both swirl numbers. This is because, in a lower concentration of CH_4, the local heat release is significantly reduced due to the less breaking bonds of carbon atoms. The rate of flame length reduction is 14% and 25% at the swirl number of 0.3 for 10% and 20% dilution respectively, and is 37% and 40% at the swirl number of 0.3 in the case of 10% and 20% fuel dilution sequentially. When CO_2 is added to the fuel stream, the flame length decreases at all swirl numbers. It should be noted that by increasing the swirl number, the rate of flame length reduction (from 0% to 10% dilution) is more noticeable at the swirl number of 0.6 meaning that mixing time decreases significantly by both dilution and swirl effects. On the other hand, the rate of flame length reduction (from 10% to 20% dilution) is more significant at the swirl number of 0.3 showing that the effect of dilution on mixing time is dominant at lower swirl intensity.

4 Conclusion

Currently, in the work being undertaken, the bluff-body swirl stabilized diffusion flame has been modeled using steady laminar flamelet model (SLFM) to investigate the effects of fuel and oxidizer CO_2 dilution on combustion characteristics. k–ω SST turbulence model is utilized to close the Reynolds stresses . Considering the computational costs, 2D axisymmetric RANS

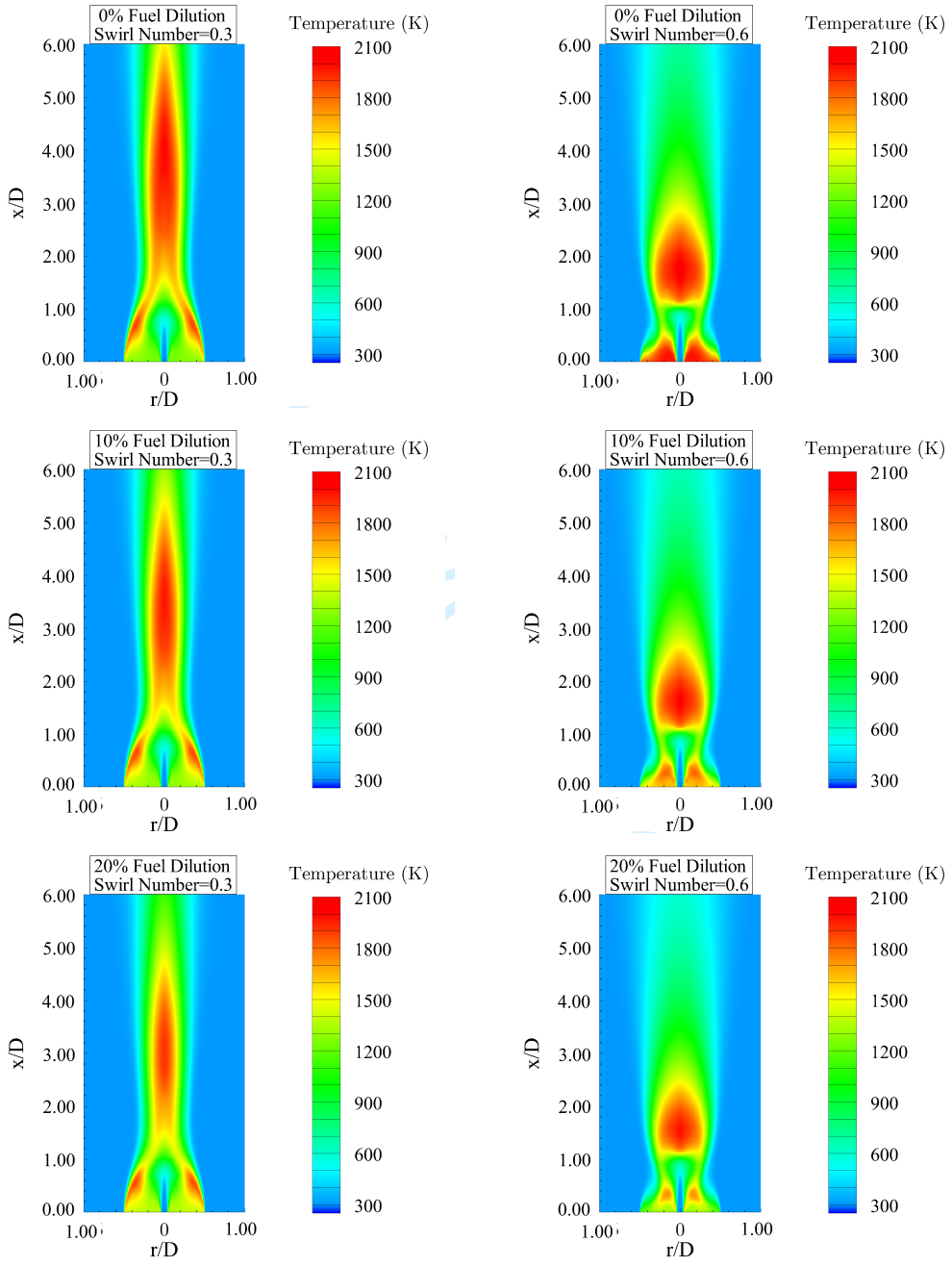

Fig. 15 The temperature contours for the cases with 0%, 10% and 20% fuel dilution and swirl numbers of 0.3 (left) and 0.6 (right).

modeling is able to capture the important features of flow and combustion field, and the results are comparable with 3D URANS simulation; however, some details of flow features are missed in comparison with 3D LES simulation. In general, the results from computational methods are consistent with measurements, and follow the main trends of variables which are of interest in the current research. In the next stage, the effects of CO_2 dilution on the flame structure, temperature distribution, flame strength, and CO mass fraction is discussed. A fictitious species was replaced by the regular CO_2 in both fuel and oxidizer streams to determine chemical effects of CO_2 dilution. The fictitious species has the similar thermal and transport properties of CO_2 however, it does not participate in chemical reactions. The results show that the flame temperature had been reduced by addition of CO_2 to the fuel and oxidizer stream. The heat capacity and endothermic thermal dissociation process of CO_2 were responsible for the decrease of flame temperature. The chain carrier radical H, which is the indicator of flame strength, also decreased due to the thermal and chemical effects of CO_2 dilution. It is the result of H atoms consumption in reaction R99 which has been introduced as the primary reaction responsible for the chemical effects of CO_2 dilution. The flame length reduction is observed in all dilution cases. In the case of fuel dilution, it is mainly related to the decrease of the combustible component of fuel which decreased mixing time. Also in the case of oxidizer dilution, the flame length was reduced due to the increase in the momentum of oxidizer flow and generation of stronger recirculation zone. CO mass fraction is affected by the amount of CO_2 dilution, flame temperature and concentration of H atoms in the reaction zone. Since the production of CO originates from CO_2 breaking down by thermal dissociation process, CO mass fraction reduced in low-temperature regions where the CO_2 dissociation has been limited. Moreover, a study on the influence of fuel dilution and swirl intensity interactions on the flame structure has been conducted. The results depicted that the swirl number variation led to considerable changes in flame structure. At low swirl number, the flame had a conical configuration at the downstream position whereas, at higher swirl number, it showed an hour-glass shape. By the addition of CO_2 to the fuel stream, the length and radius of high-temperature regions have been reduced at all swirl numbers. This is because in a lower concentration of CH_4, the breaking of carbon atom bonds decreased and it caused the reduction of local heat release. By increasing the level of dilution (from 10% to 20%) the rate of flame length reduction is more significant at low swirl number.

References

[1] T. F. Wall, Combustion processes for carbon capture, Proceedings of the combustion institute 31 (1) (2007) 31–47.

[2] A. Cavaliere, M. de Joannon, Mild combustion, Progress in Energy and Combustion science 30 (4) (2004) 329–366.

[3] D. S. Kim, C. S. Lee, Improved emission characteristics of hcci engine by various premixed fuels and cooled egr, Fuel 85 (5) (2006) 695–704.

[4] F. Liu, H. Guo, G. J. Smallwood, Ö. L. Gülder, The chemical effects of carbon dioxide as an additive in an ethylene diffusion flame: implications for soot and NOx formation, Combustion and Flame 125 (1) (2001) 778–787.

[5] J. I. Erete, K. J. Hughes, L. Ma, M. Fairweather, M. Pourkashanian, A. Williams, Effect of CO2 dilution on the structure and emissions from turbulent, non-premixed methane–air jet flames, Journal of the Energy Institute 90 (2) (2017) 191–200.

[6] J. Park, D.-J. Hwang, J.-G. Choi, K.-M. Lee, S.-I. Keel, S.-H. Shim, Chemical effects of CO2 addition to oxidizer and fuel streams on flame structure in H2–O2 counterflow diffusion flames, International journal of energy research 27 (13) (2003) 1205–1220.

[7] A. Mameri, F. Tabet, A. Hadef, Numerical investigation of biogas diffusion flames characteristics under several operation conditions in counter-flow configuration with an emphasis on thermal and chemical effects of CO2 in the fuel mixture, Heat and Mass Transfer (2017) 1–10.

[8] L. Chen, A. F. Ghoniem, Modeling CO2 chemical effects on CO formation in oxy-fuel diffusion flames using detailed, quasi-global, and global reaction mechanisms, Combustion Science and Technology 186 (7) (2014) 829–848.

[9] P. Glarborg, L. L. Bentzen, Chemical effects of a high CO2 concentration in oxy-fuel combustion of methane, Energy & Fuels 22 (1) (2007) 291–296.

[10] C. Hoerlle, L. Zimmer, F. Pereira, Numerical study of CO2 effects on laminar non-premixed biogas flames employing a global kinetic mechanism and the flamelet-generated manifold technique, Fuel 203 (2017) 671–685.

[11] S. Cao, B. Ma, D. Giassi, B. A. V. Bennett, M. B. Long, M. D. Smooke, Effects of pressure and fuel dilution on coflow laminar methane–air diffusion flames: A computational and experimental study, Combustion Theory and Modelling (2017) 1–22.

[12] D. A. Wilson, K. M. Lyons, Effects of dilution and co-flow on the stability of lifted non-premixed biogas-like flames, Fuel 87 (3) (2008) 405–413.

[13] S. Cao, B. Ma, B. Bennett, D. Giassi, D. Stocker, F. Takahashi, M. Long, M. Smooke, A computational and experimental study of coflow laminar methane/air diffusion flames: Effects of fuel dilution, inlet velocity, and gravity, Proceedings of the Combustion Institute 35 (1) (2015) 897–903.

[14] H. Watanabe, S. J. Shanbhogue, S. Taamallah, N. W. Chakroun, A. F. Ghoniem, The structure of swirl-stabilized turbulent premixed CH4/air and CH4/O2/CO2 flames and mechanisms of intense burning of oxy-flames, Combustion and Flame 174 (2016) 111–119.

[15] N. Gascoin, Q. Yang, K. Chetehouna, Thermal effects of CO2 on the NOx formation behavior in the CH4 diffusion combustion system, Applied Thermal Engineering 110 (2017) 144–149.

[16] M. Gu, H. Chu, F. Liu, Effects of simultaneous hydrogen enrichment and carbon dioxide dilution of fuel on soot formation in an axisymmetric coflow laminar ethylene/air diffusion flame, Combustion and Flame 166 (2016) 216–228.

[17] J. Park, S.-G. Kim, K.-M. Lee, T. K. Kim, Chemical effect of diluents on flame structure and NO emission characteristic in methane-air counterflow diffusion flame, International Journal of Energy Research 26 (13) (2002) 1141–1160.

[18] L. Zhuo, Y. Jiang, R. Qiu, J. An, W. Xu, Effects of fuel-side N2, CO2, H2O dilution on combustion characteristics and NOx formation of syngas turbulent nonpremixed jet flames, Journal of Engineering for Gas Turbines and Power 136 (6) (2014) 061505.

[19] L. Wang, Z. Liu, S. Chen, C. Zheng, J. Li, Physical and chemical effects of CO_2 and H_2O additives on counterflow diffusion flame burning methane, Energy & fuels 27 (12) (2013) 7602–7611.

[20] J. Min, F. Baillot, H. Guo, E. Domingues, M. Talbaut, B. Patte-Rouland, Impact of CO_2, N_2 or Ar diluted in air on the length and lifting behavior of a laminar diffusion flame, Proceedings of the Combustion Institute 33 (1) (2011) 1071–1078.

[21] H. Xu, F. Liu, S. Sun, Y. Zhao, S. Meng, W. Tang, Effects of H_2O and CO_2 diluted oxidizer on the structure and shape of laminar coflow syngas diffusion flames, Combustion and Flame 177 (2017) 67–78.

[22] N. Syred, J. Beer, Combustion in swirling flows: a review, Combustion and flame 23 (2) (1974) 143–201.

[23] R.-H. Chen, J. F. Driscoll, The role of the recirculation vortex in improving fuel-air mixing within swirling flames, in: Symposium (International) on Combustion, Vol. 22, Elsevier, 1989, pp. 531–540.

[24] R.-H. Chen, J. F. Driscoll, Nitric oxide levels of jet diffusion flames: effects of coaxial air and other mixing parameters, in: Symposium (International) on Combustion, Vol. 23, Elsevier, 1991, pp. 281–288.

[25] T. Claypole, N. Syred, The effect of swirl burner aerodynamics on NOx formation, in: Symposium (International) on Combustion, Vol. 18, Elsevier, 1981, pp. 81–89.

[26] A. Datta, S. Som, Combustion and emission characteristics in a gas turbine combustor at different pressure and swirl conditions, Applied Thermal Engineering 19 (9) (1999) 949–967.

[27] M. Day, S. Tachibana, J. Bell, M. Lijewski, V. Beckner, R. K. Cheng, A combined computational and experimental characterization of lean premixed turbulent low swirl laboratory flames: I. methane flames, Combustion and Flame 159 (1) (2012) 275–290.

[28] M. Gregor, F. Seffrin, F. Fuest, D. Geyer, A. Dreizler, Multi-scalar measurements in a premixed swirl burner using 1D Raman/Rayleigh scattering, Proceedings of the Combustion Institute 32 (2) (2009) 1739–1746.

[29] U. Stopper, W. Meier, R. Sadanandan, M. Stöhr, M. Aigner, G. Bulat, Experimental study of industrial gas turbine flames including quantification of pressure influence on flow field, fuel/air premixing and flame shape, Combustion and Flame 160 (10) (2013) 2103–2118.

[30] Y. M. Al-Abdeli, A. R. Masri, Stability characteristics and flowfields of turbulent non-premixed swirling flames, Combustion Theory and Modelling 7 (4) (2003) 731–766.

[31] T. Cheng, Y.-C. Chao, D.-C. Wu, T. Yuan, C.-C. Lu, C.-K. Cheng, J.-M. Chang, Effects of fuel-air mixing on flame structures and NOx emissions in swirling methane jet flames, in: Symposium (International) on Combustion, Vol. 27, Elsevier, 1998, pp. 1229–1237.

[32] P. A. Kalt, Y. M. Al-Abdell, A. R. Masri, R. S. Barlow, Swirling turbulent non-premixed flames of methane: flow field and compositional structure, Proceedings of the Combustion Institute 29 (2) (2002) 1913–1919.

[33] A. Masri, P. Kalt, Y. Al-Abdeli, R. Barlow, Turbulence–chemistry interactions in non-premixed swirling flames, Combustion Theory and Modelling 11 (5) (2007) 653–673.

[34] A. R. Masri, P. A. Kalt, R. S. Barlow, The compositional structure of swirl-stabilised turbulent nonpremixed flames, Combustion and Flame 137 (1-2) (2004) 1–37.

[35] T.-S. Cheng, Y.-C. Chao, D.-C. Wu, H.-W. Hsu, T. Yuan, Effects of partial premixing on pollutant emissions in swirling methane jet flames, Combustion and flame 125 (1-2) (2001) 865–878.

[36] K. P. Vanoverberghe, E. V. Van Den Bulck, M. J. Tummers, Confined annular swirling jet combustion, Combustion Science and Technology 175 (3) (2003) 545–578.

[37] J. M. Beér, N. A. Chigier, Combustion aerodynamics, New York.

[38] B. Jenkins, P. Mullinger, Industrial and process furnaces: principles, design and operation, Elsevier, 2011.

[39] A. Kempf, W. Malalasekera, K. Ranga-Dinesh, O. Stein, Large eddy simulations of swirling non-premixed flames with flamelet models: a comparison of numerical methods, Flow, turbulence and combustion 81 (4) (2008) 523–561.

[40] R. De Meester, B. Naud, U. Maas, B. Merci, Transported scalar pdf calculations of a swirling bluff body flame (sm1) with a reaction diffusion manifold, Combustion and Flame 159 (7) (2012) 2415–2429.

[41] B. Kashir, S. Tabejamaat, N. Jalalatian, A numerical study on combustion characteristics of blended methane-hydrogen bluff-body stabilized swirl diffusion flames, International Journal of Hydrogen Energy 40 (18) (2015) 6243–6258.

[42] A. Mardani, A. Fazlollahi-Ghomshi, Numerical investigation of a double-swirled gas turbine model combustor using a rans approach with different turbulence–chemistry interaction models, Energy & Fuels 30 (8) (2016) 6764–6776.

[43] A. Mardani, A. F. Ghomshi, Numerical study of oxy-fuel mild (moderate or intense low-oxygen dilution combustion) combustion for ch4–h2 fuel, Energy 99 (2016) 136–151.

[44] B. Rohani, K. M. Saqr, Effects of hydrogen addition on the structure and pollutant emissions of a turbulent unconfined swirling flame, International Communications in Heat and Mass Transfer 39 (5) (2012) 681–688.

[45] X. Yang, Z. He, S. Dong, H. Tan, Combustion characteristics of bluff-body turbulent swirling flames with coaxial air microjet, Energy & Fuels 31 (12) (2017) 14306–14319.

[46] H. Müller, F. Ferraro, M. Pfitzner, Implementation of a steady laminar flamelet model for non-premixed combustion in LES and RANS simulations, in: 8th International OpenFOAM Workshop, 2013.

[47] A. Gupta, R. Kumar, Three-dimensional turbulent swirling flow in a cylinder: Experiments and computations, International journal of Heat and fluid flow 28 (2) (2007) 249–261.

[48] F. R. Menter, M. Kuntz, R. Langtry, Ten years of industrial experience with the sst turbulence model, Turbulence, heat and mass transfer 4 (1) (2003) 625–632.

[49] L. Chen, A. F. Ghoniem, Simulation of oxy-coal combustion in a 100 kwth test facility using rans and les: a validation study, Energy & Fuels 26 (8) (2012) 4783–4798.

[50] J. Fu, Y. Tang, J. Li, Y. Ma, W. Chen, H. Li, Four kinds of the two-equation turbulence model's research on flow field simulation performance of dpf's porous media and swirl-type regeneration burner, Applied Thermal Engineering 93 (2016) 397–404.

[51] M. Safavi, E. Amani, A comparative study of turbulence models for non-premixed swirl-stabilized flames, Journal of Turbulence (2018) 1–34.

[52] T. Poinsot, D. Veynante, Theoretical and numerical combustion, RT Edwards, Inc., 2005.

[53] W. Malalasekera, K. Ranga-Dinesh, S. S. Ibrahim, A. R. Masri, Les of recirculation and vortex breakdown in swirling flames, Combustion Science and Technology 180 (5) (2008) 809–832.

[54] O. Stein, A. Kempf, Les of the sydney swirl flame series: A study of vortex breakdown in isothermal and reacting flows, Proceedings of the Combustion Institute 31 (2) (2007) 1755–1763.

[55] N. Peters, Turbulent combustion, Cambridge university press, 2000.

[56] D. G. Goodwin, H. K. Moffat, R. L. Speth, Cantera: An object-oriented software toolkit for chemical kinetics, thermodynamics, and transport processes, `http://www.cantera.org`, version 2.3.0 (2017). doi:10.5281/zenodo.170284.

[57] J. Janicka, N. Peters, Prediction of turbulent jet diffusion flame lift-off using a pdf transport equation, in: Symposium (International) on Combustion, Vol. 19, Elsevier, 1982, pp. 367–374.

[58] C. Bowman, R. Hanson, D. Davidson, W. Gardiner, V. Lissianski, G. Smith, D. Golden, M. Frenklach, M. Goldenberg, Gri-mech 2.11, 1997, URL http://www. me. berkeley. edu/gri_mech.

[59] H. G. Weller, G. Tabor, H. Jasak, C. Fureby, A tensorial approach to computational continuum mechanics using object-oriented techniques, Computers in physics 12 (6) (1998) 620–631.

[60] R. I. Issa, Solution of the implicitly discretised fluid flow equations by operator-splitting, Journal of computational physics 62 (1) (1986) 40–65.